SCIENTIFIC REPORTS

OPEN

Plasmonic refractive index sensing using strongly coupled metal nanoantennas: nonlocal limitations

Received: 11 April 2018
Accepted: 14 June 2018
Published online: 25 June 2018

Hancong Wang

Localized surface plasmon resonance based on coupled metallic nanoparticles has been extensively studied in the refractive index sensing and the detection of molecules. The amount of resonance peak-shift depends on the refractive index of surrounding medium and the geometry/symmetry of plasmonic oligomers. It has recently been found that as the feature size or the gap distance of plasmonic nanostructures approaches several nanometers, quantum effects can change the plasmon coupling in nanoparticles. However, most of the research on plasmonic sensing has been done based on classical local calculations even for the interparticle gap below ~3 nm, in which the nonlocal screening plays an important role. Here, we theoretically investigate the nonlocal effect on the evolution of various plasmon resonance modes in strongly coupled nanoparticle dimer and trimer antennas with the gap down to 1 nm. Then, the refractive index sensing in these nonlocal systems is evaluated and compared with the results in classical calculations. We find that in the nonlocal regime, both refractive index sensibility factor and figure of merit are actually smaller than their classical counterparts mainly due to the saturation of plasmon shifts. These results would be beneficial for the understanding of interaction between light and nonlocal plasmonic nanostructures and the development of plasmonic devices such as nanosensors and nanoantennas.

Surface plasmons (SP) is the collective electromagnetic (EM) excitation of conduction electrons at metal-dielectric boundary, which can induce the confinement and enhancement of electric field near the surface of noble metallic nanostructures[1]. Local SP have been exploited to manipulate light-related phenomena at the nanoscale[2,3], e.g. near-field enhancement (or "hot spot" distribution)[4–6], emission polarization[7–10], scattering direction[11], optical force[12,13], spin-orbit interaction[14], and charge transfer[15]. Many of these manipulations could be used for plasmonic sensing[16–19], stemmed from the effect of the dielectric function (or refractive index) of surrounding medium on the surface plasmon resonance (SPR)[20]. The sensing techniques using SP include: (i) surface-enhanced spectroscopys based on the amplification of the optical field at the gaps of few nanometers[4,19,21,22]; (ii) SPR sensors[16,17] including surface plasmon polaritons (SPP) sensors and localized surface plasmon resonance (LSPR) sensors[23]. Among them, the LSPR sensor has the advantage of portability involving individual plasmonic nanoparticles suspended in solutions or supported on substrates[24,25]. For a nanoscale volume of chemical/biological species adsorbed on the metal nanostructures, although the contrast in refractive index (RI) is tiny, it is still possible to induce a measurable shift of resonant peak positions[26,27].

Actually, many factors may affect the real plasmonic sensing measured in experiments, such as, (i) the *absorption effect* in particles of large size[28], (ii) the *near-field enhancement effect* because of atomistic modify of surface shape in solution due to such as the molecule functionalization[29,30], and (iii) the *size distribution effect* of nanoparticle solutions that would broaden the plasmonic resonance and decrease the figure of merit (FoM). While for the strongly coupled metal nanoparticles, as the gap distance narrows, the classical EM theory predicts an ultrahigh near-field enhancement in the gap[31–34], a diverging red shift of bonding plasmon resonance, and a strong far-field scattering. Recently, it was reported that plasmonic quantum effects, e.g. nonlocality (<3 nm) and electron tunneling (<1 nm), will emerge and drastically change the plasmonic responses for gaps approaching 1 nm[35–52]. For example, the nonlocality of the plasmon-induced screening charge might be sensitive to the refractive index of

The Fujian Provincial Key Laboratory of Automotive Electronics and Electric Drive, Research center for Microelectronics Technology, School of Information Science and Engineering, Fujian University of Technology, Fuzhou, 350108, PR China. Correspondence and requests for materials should be addressed to H.W. (email: hcwang@fjut.edu.cn)

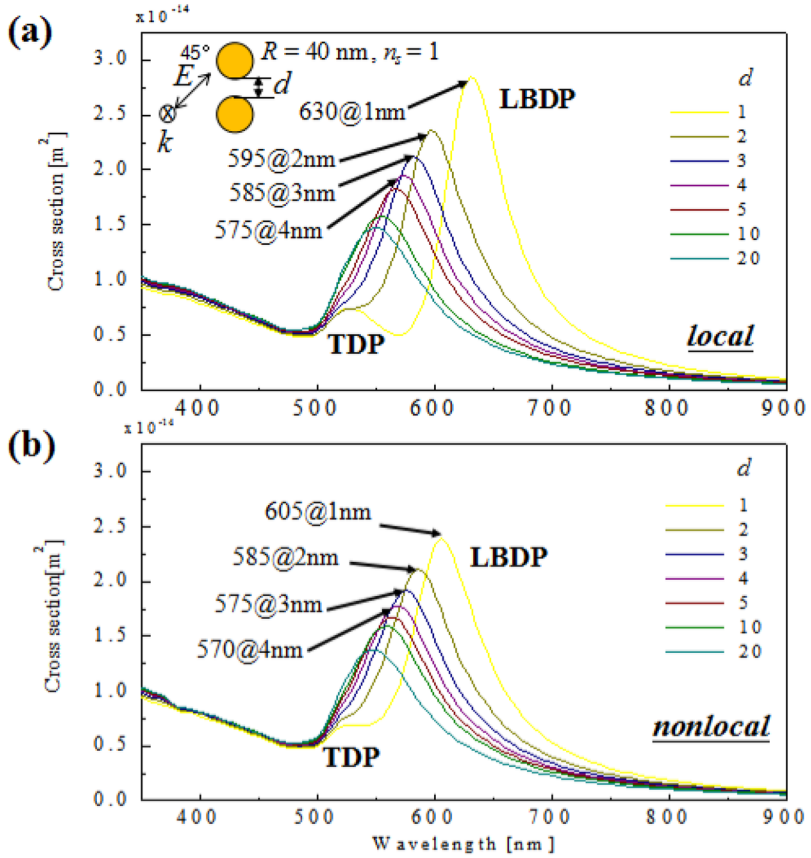

Figure 1. Scattering spectra of an individual spherical gold nanoparticle dimer with different gap distances (left to right, 20 nm to 1 nm) under a 45° polarized excitations. (**a**) Classical local prediction by GMT and (**b**) incorporating nonlocal effect by LAM. The radius of nanoparticle is R = 40 nm. Abbreviations for resonances: LBDP, longitudinal bonding dipole; TDP, transverse dipole.

surrounding media[53], especially for typical interparticle gap below ~3 nm scale (nonlocal regime)[9]. Hence, *nonlocal effect* on RI sensing should also be fully considered in strongly coupled metal nanoantennas.

In this work, we theoretically investigate the plasmon resonance evolutions and RI sensing of plasmonic nanoparticle dimer and trimer with the gap distance down to nonlocal regime. The resonance peak position and RI sensing as a function of gap and geometry/symmetry are evaluated by the generalized Mie theory (GMT)[54,55] and local analogue model (LAM)[44,45] incorporating nonlocality. In the classical regime, for the dimer, the dipolar coupling (longitudinal bonding dipole, LBDP) results in the strong dependence of resonant peak on the gap distance, while the transverse dipole mode (TDP) shows weakly dependence feature. For the trimer, the change of its symmetry will bring various evolutions of scattering peaks. As to the RI sensing, higher sensibility is found for the parallel polarized incidence. However, as the gap distance further narrows to 1~3 nm range, nonlocal effects manifests as a saturation of resonant red-shift due to the reduction of screening charge density in the gap, which reduces the RI sensibility and FoM. These results indicate the possibility of manipulating the scattering and sensing by nonlocal plasmons and developing plasmonic nanosensors and nanoantennas.

Results

Plasmon resonances of nanoantennas in nonlocal regime. Figure 1 shows the simulated scattering spectra of gold nanoparticle dimers with the interparticle gap distance decreasing from 20 nm to 1 nm. The radius of the gold sphere used in simulation is 40 nm. To mimic an unpolarized excitation, the polarization of normal incident plane wave was set as 45° relative to the longitudinal axis of dimer antennas. The RI of the surrounding medium is set to be 1. The classical local simulation shown in Fig. 1(a) is performed based on GMT (see methods for details). For large interparticle distances (10~20 nm), the EM coupling between nanoparticles is weak. In this situation, the LBDP mode generated by two nanoparticles interaction is close to the uncoupled TDP mode that mainly contributes from single nanoparticle dipolar resonance. Actually, the interaction energy between two nanoparticles can be expressed by: $V \sim p_1 * p_2/d^3$, where p indicates the dipole moments of a single nanoparticle and d is the gap distance[1]. Obviously, the interaction energy will dramatically increase with the decrease of distance. As shown in Fig. 1(a), the LBDP significantly red-shifts from 540 nm to 630 nm when the interparticle distance decreases from 20 nm to 1 nm, while the uncoupled TDP mode shows little dependence on the distance.

However, as the feature size approaches to ~1 nm scale, the screening charge smear out due to the finite Fermi wavelength of electrons. This spatial dispersion (nonlocality) has a large impact on the optical response[38]. The

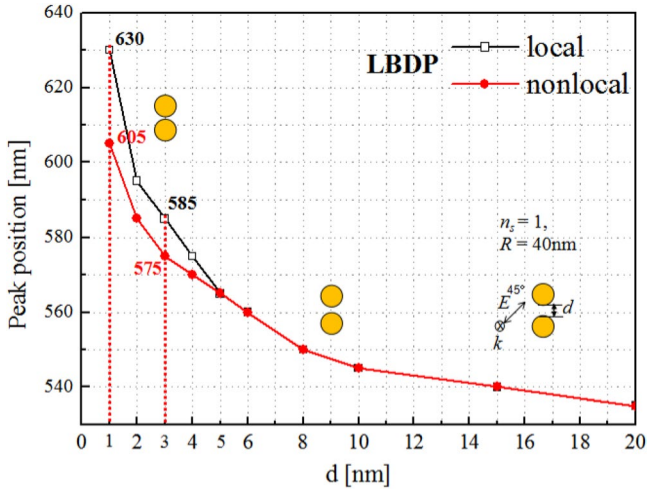

Figure 2. LBDP peak positions as a function of gap distances. Local prediction by GMT (black hollow squares) and results incorporating nonlocal effect by LAM (red solid circles). The lines are plotted to guide eyes.

dielectric permittivity in nonlocal regime depends on both the frequency and electron wavenumber. This correction is important for very small gaps less than 3 nm. Hence, we further performed the simulation using local analogue model (LAM) to incorporate the nonlocality into the local EM framework (see Methods for details). The nonlocal LBDP in Fig. 1(b) obviously shows less red shift than local case in Fig. 1(a) when the distance decreases from 3 nm to 1 nm.

Figure 2 summarizes the evolution of peak positions of LBDP modes as a function of the gap distance by local and nonlocal models. It is found that, when the distance is larger than ~3 nm, the nonlocal simulation almost agrees with the local one. However, as the distance is smaller than ~3 nm, the nonlocal result (red solid circles in Fig. 2) begins to deviate from the local prediction (black hollow squares in Fig. 2), showing less red shift than the local one. At $d = 3$ nm, the discrepancy of red shifts between the nonlocal and local cases is about 10 nm, which indicates that the nonlocal effect begins to play an important role. For a smaller gap, the discrepancy become larger. At $d = 1$ nm, the discrepancy is as large as 25 nm.

Plasmonic sensing using strongly coupled dimer nanoantennas. Besides the gap distance, another important parameter influencing SP coupling is the dielectric environment[25]. Actually, the plasmonic sensitivity is strongly dependent on the size, shape, composition, and structure of nanostructrues[56]. Therefore, plasmonic nanoparticles are ideal platforms for refractive index sensing. In the following, we will discuss the nonlocal effect on the sensing properties of plasmonic nanoparticle dimer and trimers. Figure 3(a,b) show the simulated local and nonlocal scattering spectra of a gold dimer with the gap distance $d = 1$ nm under the parallel (90°) incident polarization, respectively. The environmental refractive index $n_s = 1$, 1.33, and 1.65 are represented by blue, green, and red curves, respectively. For local dimers in Fig. 3(a), the LBDP peak red-shifts significantly with the increasing of n_s due to the strong near-field plasmonic coupling between two nanoparticles under the parallel polarization. From $n_s = 1$ to 1.65, the LBDP mode almost linearly red-shifts from 630 nm to 910 nm. The multipole modes (MP) in shorter wavelength region can also be excited under the parallel polarized excitation. Different from the LBDP mode, the multipole mode slightly red-shifts from 530 nm to 650 nm. For the nonlocal dimers in Fig. 3(b), on the other hand, the magnitude of LBDP mode red shift is reduced. Correspondingly, from $n_s = 1$ to 1.65, the nonlocal LBDP mode red-shifts from 605 nm to 815 nm. While, the nonlocal effect has less influence on the multipole mode. The corresponding multipole peaks are from 530 nm to only 590 nm.

Then, we can analyze the sensing properties of dimers under the local and nonlocal cases. The resonance wavelength sensitivity factor S is usually used to quantify the performance of RI sensing, defined as the peak shift per unit change in the surrounding refractive index (RIU)[23]. This RI sensitivity factor for local LBDP is about $S \approx 431$ nm/RIU that decrease to 323 nm/RIU for nonlocal case, which is about 25.1% reduction relative to the local prediction.

As to the peak width, in analogy to a damped oscillator, the peak width is directly related to its decay time, which in turn is determined by the damping of SP. The effect of peak width on sensing is typically evaluated by the FoM[24], which is defined as the ratio of sensitivity factor S to scattering peak linewidth (FWHM, Full width at half maximum) $\Delta\lambda$, that is, $\text{FoM} = S/\Delta\lambda$. Actually, the modal linewidth can also be largely affected by nonlocality through surface-enhanced Landau damping, an effect that can be efficiently captured by the nonlocal optical response theory applied for instance in refs[35,48], predicting drastic broadening of the plasmon modes. Here, for $n_s = 1.33$, the FoM of the dimer is about 3.6 and reduced to 2.7 if the nonlocal effect is considered. We find both the RI sensitivity factor and FoM are larger than their nonlocal counterparts due to more obvious plasmon shifts in local simulations. For the multipole modes, however, there are less difference between the local and nonlocal regime. Also, the angle of incident polarization dramatically changes the coupling and then the sensitivity of a dimer.

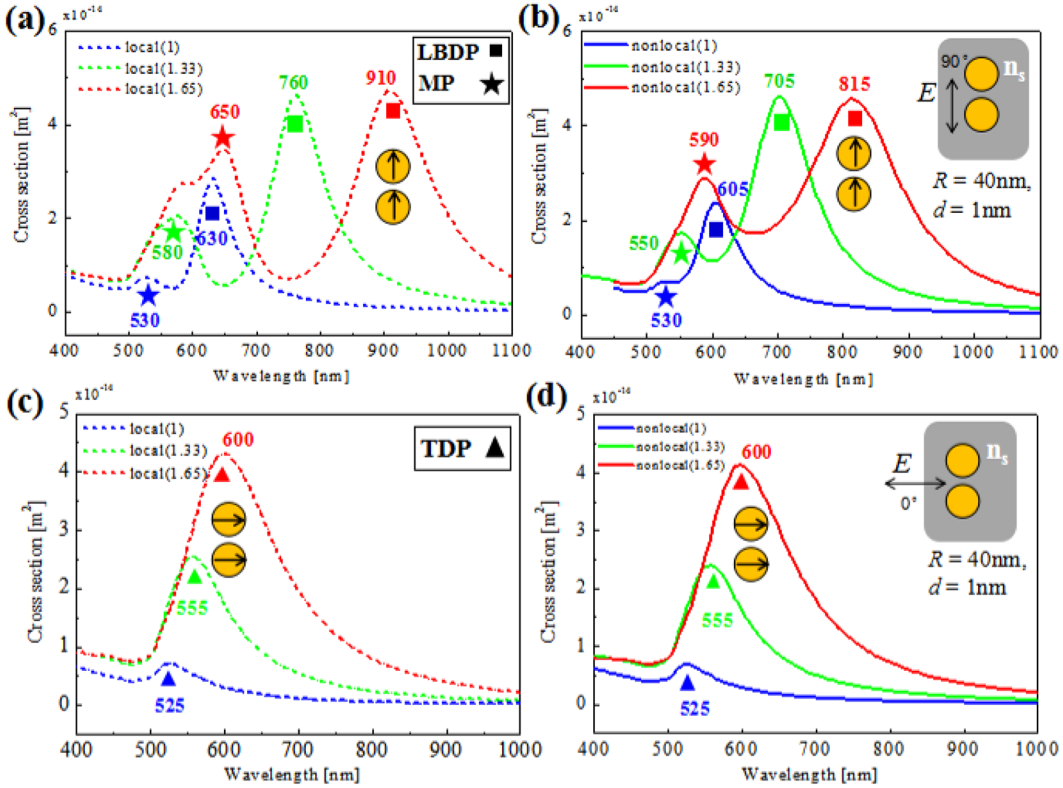

Figure 3. Scattering spectra of a dimer with different environmental refractive index n_s. (**a**) Local and (**b**) nonlocal cases with parallel polarized excitation, respectively. (**c**) Local and (**d**) nonlocal cases with perpendicular polarized excitation, respectively. Blue, green, and red curves correspond to refractive index $n_s = 1$, 1.33, and 1.65, respectively.

Figure 3(c,d) show the simulated local and nonlocal scattering spectra for the perpendicular (0°) incident polarization, respectively. Here, only the TDP mode can be excited. For TDP mode, its sensitivity factor S is 115 nm/RIU for both the local and nonlocal ones. As the RI sensitivity and nonlocality shows less influence on the uncoupled mode, we will mainly focus on the coupled modes in the trimer case.

Plasmonic sensing using strongly coupled trimer nanoantennas. We consider two kinds of typical configurations, that is, linear trimer and right-angle (asymmetric) trimer. As shown in Fig. 4, the linear trimer (symmetry point group $D_{\infty h}$) or a right-angle trimer (group C_{2v}) are formed by positioning a same particle on the top or right side of the 2nd one[6,57–59]. Here, all the gaps between any two closely packed particles are 1 nm. Based on the plasmon hybridization (PH) theory[60] and symmetry adopted linear combination (SALC) theory[57,58], the main plasmon modes are $\sum^+_u$, $\prod_u$ modes for $D_{\infty h}$ trimer, and B_2, A_1 modes for C_{2v} trimer. The linear trimer case with the polarization parallel to the trimer axis are shown in Fig. 4(a,b), where a strong coupled low-energy $\sum^+_u$ mode and a weak high-energy multipole mode are excited. In the local regime in Fig. 4(a), both modes red-shift as the increasing RI. From $n_s = 1$ to 1.65, the $\sum^+_u$ mode red-shifts from 685 nm to 1040 nm. The RI sensitivity factor of $\sum^+_u$ peak is about $S \approx 546$ nm/RIU. This value is larger than the LBDP mode in dimer case. While for the nonlocal regime in Fig. 4(b), the $\sum^+_u$ mode red-shifts from 655 nm to 925 nm, corresponding to a RI sensitivity factor $S \approx 415$ nm/RIU, which is about 24.0% reduction relative to the local prediction. The nonlocality caused-reduction of RI sensitivity in the linear trimer is slightly less than the dimer case. For $n_s = 1.33$, the FoM is about 3.2 (local) or 2.3 (nonlocal). Both RI sensitivity factor and FoM are smaller than their local cases due to the more obvious resonance shifts in classical simulations.

Figure 4(c,d) show the right-angle trimer (group C_{2v}) with the polarization parallel to the dimer axis (1st–2nd). The strong coupled low-energy B_2 mode and a weak high-energy multipole mode are excited. Similar to previous analysis, the classical local RI sensitivity for B_2 mode is about 469 nm/RIU, which is reduced to 361 nm/RIU for the nonlocal case. For $n_s = 1.33$, the FoM is about 3.6 (local) or 2.6 (nonlocal). Because of its narrower width of resonance, the C_{2v} trimer has higher FoM than the case of $D_{\infty h}$ trimer.

Discussion

To compare the RI sensitivities of different plasmon modes in nanoparticle antennas, we plot resonant peaks as a function of the environmental refractive index for four modes, including LBDP and TDP modes in dimer, $\sum^+_u$ modes in $D_{\infty h}$ trimer, and B_2 modes in C_{2v} trimer. As shown in Fig. 5, the shift of all modes is approximately linear to the change of refractive index. The gradients for each line are the RI sensitivities which are summarized in

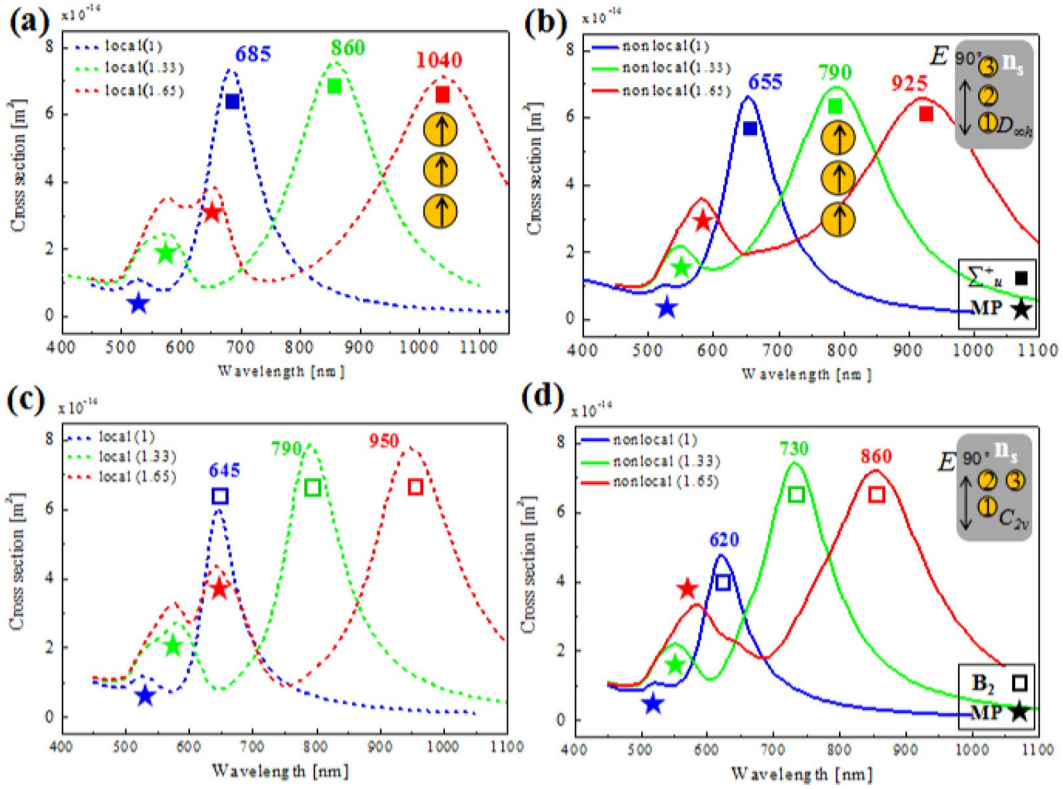

Figure 4. Scattering spectra of trimers with different environmental refractive index n_s under parallel polarization excitations. (**a**) Local and (**b**) nonlocal cases for linear timer, respectively. (**c**) Local and (**d**) nonlocal cases for right-angle trimer, respectively. Blue, green, and red curves correspond to refractive index $n_s = 1$, 1.33, and 1.65, respectively.

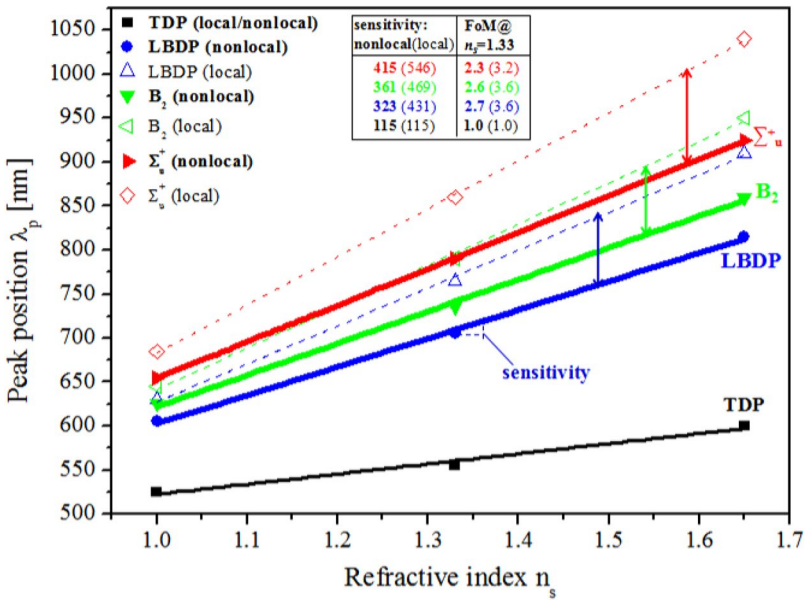

Figure 5. The nonlocal (solid lines) and local (dashed lines) resonance peak positions λ_p as a function of the environmental refractive index n_s for different modes. $\sum^{+}{}_{u}$ mode (red) in $D_{\infty h}$ trimer, B_2 mode (green) in C_{2v} trimer, LBDP mode (blue) and TDP mode (black) in dimer. RI sensitivities (slope) are obtained using a linear fitting. The inset box lists RI sensitivities and FoMs calculated by nonlocal and local models. FoMs are calculated at $n_s = 1.33$.

the inset box in Fig. 5. Obviously, the nonlocal effect would reduce the RI sensitivity factor and FoM in all cases. Hence, for closed packed nanoparticles with the gap below ~3 nm, the nonlocal effect cannot be neglected.

In conclusion, we have investigated the scattering spectrum, RI sensitivity factor and FoM in plasmonic nanoparticle dimer and trimer antennas calculated within a local and a nonlocal framework. By comparing local and nonlocal results, it is shown that the classical local model works for the gap larger than 3 nm. As the gap further decreases to the nonlocal regime ($<\sim$3 nm), the red shift of LBDP peak positions are not significant compared with local calculations. The evolution of various surface plasmon peaks is related to gap distance, the symmetry of plasmonic nanoparticles, and especially environmental refractive index. The scattering from plasmon modes in nanoparticles can be used for refractive index sensing. A higher RI sensibility and figure of merit are found in dimer for parallel polarized excitations due to strong plasmonic coupling. Because of less plasmonic shifts, both the RI sensitivity factor and FoM of dimer and trimer nanoantennas in the nonlocal regime are smaller than their local ones. These results somehow advance the understanding on the cross-over between local and nonlocal regimes, and would be beneficial for the study of nonlocal effect on the emission from nanoantennas and the development of plasmonic nanosensors[61].

Methods

Classical Electromagnetic Calculation. The classical local simulation is performed based on the analytical Generalized Mie theory (GMT), where incident and scattered electric fields are expanded into vector spherical harmonics. The expansion coefficients of incident field are Mie coefficients. The relation between the incidence and multiple scattering is solved by the order of scattering method. Then the scattering cross section can be obtained by the summation of the square of scattering coefficients of different order. The dielectric data of gold are from the work of Johnson and Christy[62].

Local Analogue Model. The nonlocal smearing of surface charges in local analogue model (LAM)[44,45] is mapped into a thin dielectric layer Δl on top of the metal surface with permittivity ε_s. The shifting of the metal boundary is $\Delta l(\omega) = \varepsilon_s \lambda(\omega)\, \varepsilon_M(\omega)/[\varepsilon_M(\omega) + 1]$, where $\varepsilon_M(\omega)$ is the permittivity of metal core, and $\lambda(\omega)$ is the penetration depth of surface charges, which can be written as $\lambda(\omega) = \sqrt{3/5}\, V_F/\sqrt{{\omega_P}^2/\varepsilon_M(\infty) - \omega(\omega + i\gamma_{gold})}$. Here, v_F, ω_p, and $\gamma_{gold} = 0.09$ eV are the Fermi velocity, the bulk plasma frequency, and the damping frequency of gold, respectively. The Δl can be obtained by letting the shell dielectric function ε_s equal to the dielectric function of surrounding medium. It should be noted that the modeling thin layer is inside the metal, meaning the gap distance is not affected. By combining LAM with GMT for multiple core/shell particles, scattering spectra incorporating nonlocal effects can be obtained.

References

1. Halas, N. J., Lal, S., Chang, W.-S., Link, S. & Nordlander, P. Plasmons in Strongly Coupled Metallic Nanostructures. *Chem. Rev.* **111**(6), 3913–3961 (2011).
2. Li, Z. & Xu, H. Nanoantenna effect of surface-enhanced Raman scattering: managing light with plasmons at the nanometer scale. *Adv. Phys.: X* **1**(3), 492–521 (2016).
3. Giannini, V., Fernandez-Dominguez, A. I., Heck, S. C. & Maier, S. A. Plasmonic nanoantennas: fundamentals and their use in controlling the radiative properties of nanoemitters. *Chem. Rev.* **111**(6), 3888–3912 (2011).
4. Xu, H., Bjerneld, E. J., Käll, M. & Börjesson, L. Spectroscopy of Single Hemoglobin Molecules by Surface Enhanced Raman Scattering. *Phys. Rev. Lett.* **83**(21), 4357–4360 (1999).
5. Xu, H., Aizpurua, J., Käll, M. & Apell, P. Electromagnetic contributions to single-molecule sensitivity in surface-enhanced Raman scattering. *Phys. Rev. E* **62**(3), 4318–4324 (2000).
6. Wang, H., Li, Z., Zhang, H., Wang, P. & Wen, S. Giant local circular dichroism within an asymmetric plasmonic nanoparticle trimer. *Sci. Rep.* **5**, 8207 (2015).
7. Shegai, T. *et al*. Managing light polarization via plasmon-molecule interactions within an asymmetric metal nanoparticle trimer. *Proc. Natl. Acad. Sci. USA* **105**(43), 16448–16453 (2008).
8. Li, Z., Shegai, T., Haran, G. & Xu, H. Multiple-Particle Nanoantennas for Enormous Enhancement and Polarization Control of Light Emission. *ACS Nano* **3**(3), 637–642 (2009).
9. Yang, L., Wang, H., Fang, Y. & Li, Z. Polarization State of Light Scattered from Quantum Plasmonic Dimer Antennas. *ACS Nano* **10**(1), 1580–1588 (2016).
10. Yang, L., Li, P. & Li, Z. Emitting-polarization of surface plasmons coupling in metallic nanoantennas. *J. Optics-UK* **20**(1), 014002 (2018).
11. Shegai, T. *et al*. A bimetallic nanoantenna for directional colour routing. *Nat. Commun.* **2**(1), 481 (2011).
12. Xu, H. & Käll, M. Surface-Plasmon-Enhanced Optical Forces in Silver Nanoaggregates. *Phys. Rev. Lett.* **89**(24), 246802 (2002).
13. Li, Z. *et al*. Ultrasensitive Size-Selection of Plasmonic Nanoparticles by Fano Interference Optical Force. *ACS Nano* **8**(1), 701–708 (2013).
14. Pan, D., Wei, H., Gao, L. & Xu, H. Strong Spin-Orbit Interaction of Light in Plasmonic Nanostructures and Nanocircuits. *Phys. Rev. Lett.* **117**(16), 166803 (2016).
15. Wang, H. *et al*. Enhancing the saturable absorption and carrier dynamics of graphene with plasmonic nanowires. *Phys. Status Solidi B* **252**(10), 2159–2166 (2015).
16. Mayer, K. M. & Hafner, J. H. Localized Surface Plasmon Resonance Sensors. *Chem. Rev.* **111**(6), 3828–3857 (2011).
17. Tong, L., Wei, H., Zhang, S. & Xu, H. Recent advances in plasmonic sensors. *Sensors* **14**(5), 7959–7973 (2014).
18. Stewart, M. E. *et al*. Nanostructured Plasmonic Sensors. *Chem. Rev.* **108**(2), 494–521 (2008).
19. Willets, K. A. & Van Duyne, R. P. Localized surface plasmon resonance spectroscopy and sensing. *Annu. Rev. Phys. Chem.* **58**(1), 267–297 (2007).
20. Zhang, S., Bao, K., Halas, N. J., Xu, H. & Nordlander, P. Substrate-induced Fano resonances of a plasmonic nanocube: a route to increased-sensitivity localized surface plasmon resonance sensors revealed. *Nano Lett.* **11**(4), 1657–1663 (2011).
21. Jain, P. K., Huang, W. & El-Sayed, M. A. On the Universal Scaling Behavior of the Distance Decay of Plasmon Coupling in Metal Nanoparticle Pairs: A Plasmon Ruler Equation. *Nano Lett.* **7**(7), 2080–2088 (2007).
22. Lee, H., Lee, J. H., Jin, S. M., Suh, Y. D. & Nam, J. M. Single-Molecule and Single-Particle-Based Correlation Studies between Localized Surface Plasmons of Dimeric Nanostructures with approximately 1 nm Gap and Surface-Enhanced Raman Scattering. *Nano lett.* **13**(12), 6113–6121 (2013).

23. Homola, J. Surface Plasmon Resonance Sensors for Detection of Chemical and Biological Species. *Chem. Rev.* **108**(2), 462–493 (2008).
24. Sherry, L. J. *et al*. Localized surface plasmon resonance spectroscopy of single silver nanocubes. *Nano Lett.* **5**(10), 2034–2038 (2005).
25. Xia, Y. & Halas, N. J. Shape-Controlled Synthesis and Surface Plasmonic Properties of Metallic Nanostructures. *MRS Bull.* **30**(5), 338–348 (2005).
26. Lal, S., Link, S. & Halas, N. J. Nano-optics from sensing to waveguiding. *Nat. Photon.* **1**(11), 641–648 (2007).
27. Anker, J. N. *et al*. Biosensing with plasmonic nanosensors. *Nat. Mater.* **7**(6), 442–453 (2008).
28. Chen, H., Kou, X., Yang, Z., Ni, W. & Wang, J. Shape- and size-dependent refractive index sensitivity of gold nanoparticles. *Langmuir.* **24**(10), 5233–5237 (2008).
29. Barbry, M. *et al*. Atomistic near-field nanoplasmonics: reaching atomic-scale resolution in nanooptics. *Nano Lett.* **15**(5), 3410–3419 (2015).
30. Urbieta, M. *et al*. Atomic-scale lightning rod effect in plasmonic picocavities: a classical view to a quantum effect. *ACS Nano* **12**(1), 585–595 (2018).
31. Fan, J. A. *et al*. Self-assembled plasmonic nanoparticle clusters. *Science* **328**(5982), 1135–1138 (2010).
32. Lee, H. *et al*. Quantitative Plasmon Mode and Surface-Enhanced Raman Scattering Analyses of Strongly Coupled Plasmonic Nanotrimers with Diverse Geometries. *Nano lett.* **15**(7), 4628–4636 (2015).
33. Su, K. H. *et al*. Interparticle Coupling Effects on Plasmon Resonances of Nanogold Particles. *Nano Lett.* **3**(8), 1087–1090 (2003).
34. Romero, I., Aizpurua, J. & Bryant, G. W. & García de Abajo, F. J. Plasmons in nearly touching metallic nanoparticles: singular response in the limit of touching dimers. *Opt. Express* **14**(21), 9988–9999 (2006).
35. Raza, S., Bozhevolnyi, S. I., Wubs, M. & Mortensen, N. A. Nonlocal optical response in metallic nanostructures. *J. Phys-Condens. Mat.* **27**(18), 183204 (2015).
36. Tame, M. S. *et al*. Quantum plasmonics. *Nat. Phys.* **9**(6), 329–340 (2013).
37. Zhu, W. *et al*. Quantum mechanical effects in plasmonic structures with subnanometre gaps. *Nat. Commun.* **7**, 11495 (2016).
38. David, C. & de Abajo, G. F. J. Spatial Nonlocality in the Optical Response of Metal Nanoparticles. *J. Phys. Chem. C* **115**(40), 19470–19475 (2011).
39. Mao, L., Li, Z., Wu, B. & Xu, H. Effects of quantum tunneling in metal nanogap on surface-enhanced Raman scattering. *Appl. Phys. Lett.* **94**(24), 243102 (2009).
40. Zuloaga, J., Prodan, E. & Nordlander, P. Quantum Description of the Plasmon Resonances of a Nanoparticle Dimer. *Nano Lett.* **9**(2), 887–891 (2009).
41. Esteban, R., Borisov, A. G., Nordlander, P. & Aizpurua, J. Bridging quantum and classical plasmonics with a quantum-corrected model. *Nat. Commun.* **3**(3), 825 (2012).
42. Esteban, R. *et al*. A classical treatment of optical tunneling in plasmonic gaps: extending the quantum corrected model to practical situations. *Faraday Discuss.* **178**(34), 151–183 (2015).
43. Toscano, G. *et al*. Resonance shifts and spill-out effects in self-consistent hydrodynamic nanoplasmonics. *Nat. Commun.* **6**, 7132 (2015).
44. Luo, Y., Fernandez-Dominguez, A. I., Wiener, A., Maier, S. A. & Pendry, J. B. Surface Plasmons and Nonlocality: A Simple Model. *Phys. Rev. Lett.* **111**(9), 093901 (2013).
45. Luo, Y., Zhao, R. K. & Pendry, J. B. van der Waals interactions at the nanoscale: The effects of nonlocality. *Proc. Natl. Acad. Sci. USA* **111**(52), 18422–18427 (2014).
46. García de Abajo., F. J. Nonlocal Effects in the Plasmons of Strongly Interacting Nanoparticles, Dimers, and Waveguides. *J. Phys. Chem. C* **112**(46), 17983–17987 (2008).
47. Teperik, T. V., Nordlander, P., Aizpurua, J. & Borisov, A. G. Robust Subnanometric Plasmon Ruler by Rescaling of the Nonlocal Optical Response. *Phys. Rev. Lett.* **110**(26), 263901 (2013).
48. Tserkezis, C., Maack, J. R., Liu, Z., Wubs, M. & Mortensen, N. A. Robustness of the far-field response of nonlocal plasmonic ensembles. *Sci. Rep.* **6**, 28441 (2016).
49. Savage, K. J. *et al*. Revealing the quantum regime in tunnelling plasmonics. *Nature* **491**(7425), 574–577 (2012).
50. Scholl, J. A., García-Etxarri, A., Koh, A. L. & Dionne, J. A. Observation of quantum tunneling between two plasmonic nanoparticles. *Nano lett.* **13**(2), 564–569 (2013).
51. Zhu, W. & Crozier, K. B. Quantum mechanical limit to plasmonic enhancement as observed by surface-enhanced Raman scattering. *Nat. Commun.* **5**, 5228–5235 (2014).
52. Lerch, S. & Reinhard, B. M. Quantum Plasmonics: Optical Monitoring of DNA-Mediated Charge Transfer in Plasmon Rulers. *Adv. Mater.* **28**(10), 2030–2036 (2016).
53. Raza, S., Toscano, G., Jauho, A. P., Mortensen, N. A. & Wubs, M. Refractive-Index Sensing with Ultrathin Plasmonic Nanotubes. *Plasmonics* **8**(2), 193–199 (2013).
54. Xu, H. A new method by extending Mie theory to calculate local field in outside/inside of aggregates of arbitrary spheres. *Phys. Lett. A* **312**(5–6), 411–419 (2003).
55. Li, Z. & Xu, H. Electromagnetic energy flow near metal nanoparticles - II: Algorithms for the calculation of the light scattering of multi-spheres and photon energy transport via linear chains of Ag nanoparticles. *J Quant. Spectrosc. Ra.* **103**(2), 394–401 (2007).
56. Špačková, B., Wrobel, P., Bocková, M. & Homola, J. Optical Biosensors Based on Plasmonic Nanostructures: A Review. *P. IEEE* **104**(12), 2380–2408 (2016).
57. Chuntonov, L. & Haran, G. Trimeric plasmonic molecules: the role of symmetry. *Nano Lett.* **11**(6), 2440–2445 (2011).
58. Chuntonov, L. & Haran, G. Maximal Raman optical activity in hybrid single molecule-plasmonic nanostructures with multiple dipolar resonances. *Nano Lett.* **13**(3), 1285–1290 (2013).
59. Lu, G. *et al*. Directional side scattering of light by a single plasmonic trimer. *Laser Photonics Rev.* **9**(5), 530–537 (2015).
60. Prodan, E., Radloff, C., Halas, N. J. & Nordlander, P. A hybridization model for the plasmon response of complex nanostructures. *Science* **302**(5644), 419–422 (2003).
61. Xu, H. *Nanophotonics - Manipulating Light with Plasmons* (Pan Stanford Publishing, 2017).
62. Johnson, P. B. & Christy, R. W. Optical Constants of the Noble Metals. *Phys. Rev. B* **6**(12), 4370–4379 (1972).

Acknowledgements

Hancong Wang thanks Prof. Zhipeng Li and Prof. Longkun Yang for fruitful discussions. This work is financially supported by the Mid-youth Project of Education Bureau of Fujian Province (JAT160331) and the Startup Foundation for New Faculty of Fujian University of Technology (GY-Z160049).

Additional Information

Competing Interests: The author declares no competing interests.

Publisher's note: Springer Nature remains neutral with regard to jurisdictional claims in published maps and institutional affiliations.